Architectural Intelligence

RESEARCH ARTICLE

Open Access

Space-filling and print path generation methods for large-area 3D concrete printing pavements

Shuyi Huang[1], Weiguo Xu[1,2*] and Hanyang Hu[1]

Abstract

3D concrete printing (3DCP) technology is a construction method that offers a unique combination of automation and customization. However, when the printing area goes large, generating the print path becomes a sophisticated work. That's because the customized print path should not only be expandable but also printable, such rules are hard to follow as both the printing area and construction requirements increase. In this paper, the Shenzhen Baoan 3D Printing Park project serves as a case study to introduce space-filling and print path generation methods for three types of large-area concrete pavement. The space-filling methods utilize geometry-based rules to generate complex and expandable paving patterns, while the print path generation methods utilize construction-oriented rules to convert these patterns into print paths. The research provides easy-to-operate design and programming workflows to achieve a pavement printing area of 836 sqm, which significantly increases the construction scale of large-format additive manufacturing (LFAM) and shows the potential of 3D printing technology to reach non-standard results by using standard workflows.

Keywords 3D concrete printing, Large-format additive manufacturing, Space-filling, Print path generation, Robotic arms

1 Introduction

1.1 Background

3D concrete printing technology can simultaneously meet the needs of customized design and autonomous construction, and it is an important approach to solving the labor shortage problem in the current construction industry. By using a robot instead of a human to deposit the fast-setting concrete and complete construction tasks, 3DCP technology can improve construction efficiency and site safety. Additionally, benefiting from the flexibility and precision of the robot, 3D printing technology can achieve complex and unique components in the equal time it takes to build regular shapes, without requiring manual involvement to build formwork.

However, it is still challenging to apply 3DCP technology in large-area projects, as the print path is hard to meet both the increasing construction size and the limited workspace of robots. Although various mobile printers are now available for in-situ constructions (Huang et al., 2022), they can only work on flat ground and is not capable of printing on complex topography. Hence, in large construction sites with height differences, repositioning the heavy in-situ printers can be a sophisticated task. A more practical alternative is to subdivide the project into printable pieces for a single robot, which corresponds to more programming work. Moreover, in projects with high design complexity, it can be time-consuming to generate the print paths for all the unique components. Hence, there is a high demand for efficient

*Correspondence:
Weiguo Xu
xwg@mail.tsinghua.edu.cn
[1] School of Architecture, Tsinghua University, Beijing 100084, China
[2] Institute of Future Human Habitats, Shenzhen International Graduate School, Tsinghua University, Shenzhen 518055, China

and repeatable print path generation rules to confront the challenges brought by the printing size and design complexity.

1.2 Objective

This study investigates space-filling and print path generation methods for large-area 3D printed concrete pavements based on the Shenzhen Baoan 3D Printing Park project. The park spans 5,523 sqm, with a pavement area of 836 sqm - significantly larger than the current large-scale 3DCP projects, which typically cover less than 150 sqm and a maximum of about 450 sqm (Huang et al., 2022). In this project, the particle swarm optimization and strange attractor algorithm are adopted to generate the masterplan (Ruelle & Takens, 1971; Xu et al., 2022), which also defines three pavement types: river pavement for the central square and main pathway (304 sqm), coral pavement for the landscape trail (487 sqm), and cloud pavement for the sign sculpture trail (45 sqm) (Fig. 1).

When it comes to such large-area construction projects, 3D printing's advantages in mass customization can better tailor to the diverse design needs compared with mass production methods (Hu, 2013). In mass production, since pavers are produced by identical and reusable formworks, designers have to choose the paver type within the given options, which limits the versatility of design and reduces the options for potentially more sustainable, material-saving solutions (Anton et al., 2021). Moreover, large-area landscape design usually has an undulating topography, so the mass-produced pavers have to be small enough to fit the topography perfectly, meaning more human involvement in the paving process. In contrast, by using 3D printing technology, designers can customize paving patterns to meet different landscape design requirements (e.g., varying the cell size of permeable pavements, or creating concrete patterns that can be filled with other materials). Robotic arms can also help to survey the topography and print the pavement that matches the ground.

In order to achieve the above benefits of mass customization, two research questions for large-scale 3D printing are highlighted as follows:

(1) How to cover large pavement areas with regular but complex patterns?
(2) How to transform complex paving patterns into practical print paths?

The objective of this paper is to utilize easy-to-operate methods to generate the print path for large and complex paving patterns. Section 2 provides an overview of related studies and methods in building-scale LFAM. Section 3 introduces the generation method of space-filling curves for the park project. Section 4 explains how these curves can be transformed into print paths suitable for 3DCP practices. Finally, in Sections 5 and 6, we present, discuss, and summarize the results of our construction efforts.

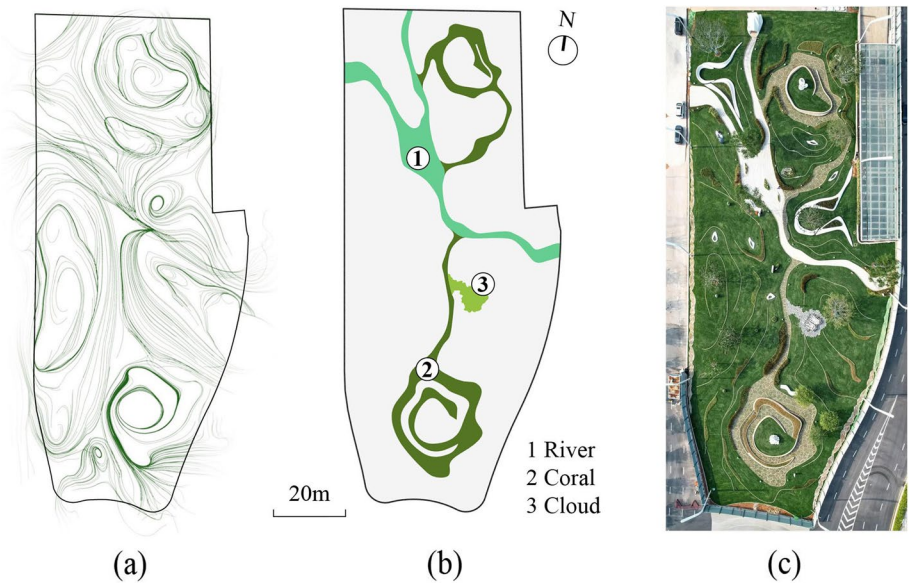

Fig. 1 The generation diagram, pavements location, and construction outcome of the Shenzhen Baoan 3D Printing Park (Sources: XWG Design Studio): (1) The reference curve for the masterplan, generated by the strange attractor algorithm; (2) The locations of three pavement types; (3) The bird's-eye view of the park

2 Literature review

The literature review consists of two parts. The first part is the research on the previous large-scale 3D printing methods to clarify the specialty of this project's research questions. The second part introduces the methodologies adopted in this study to achieve mass customization of 3DCP pavements, including various types of space-filling curves and print path generation rules.

2.1 Related works in LFAM

Large-format additive manufacturing refers to a 3D printing method in which the working area of the printing equipment is much larger than the size of the printing head. This concept was initially used to solve the volume limitations of desktop printers (Shen et al., 2019) and has now been extended to the architectural scale. Compared to desktop 3D printing, LFAM for architecture and landscape projects needs to consider topography conditions and construction costs, which cannot be realized by simply increasing the number and volume of printers (Duty et al., 2017; Krishnamurthy et al., 2022). A more practical approach is to divide the structure into multiple components that fit the printing range of the printer, and then print and transport these components to the construction site for installation (Grasser et al., 2020; Wu et al., 2022a).

A criterial research question of architectural scale LFAM is how to divide and convert the structure into transportable, printable, and easy-to-assemble components. In projects with design complexity, it is not easy to meet all these requirements. Designers must effectively subdivide complex geometries through practical approaches (Yuan et al., 2022a) and then apply standard rules to convert each customized component into print paths. Besides, these print paths need to allow the material to just fill the entire surface of the component without overfitting and underfitting areas, ensuring the quality of the printing outcome (Bi et al., 2022; Biegler et al., 2020; Wan et al., 2022).

This study is unique in its utilization of 3DCP to create pavements that not only cover a large area but also integrate with the surrounding landscape. Unlike regular LFAM, the 3DCP pavement requires a print path that forms a porous shape within each component rather than attempting to fill all the available space. In other words, the print path itself needs to be an aesthetically pleasing pattern, rather than just a space filler (Fig. 2). Therefore, the common space-filling methods for LFAM, such as contour-parallel path and zigzag path, are not suitable for this project.

2.2 Adopted methodologies

2.2.1 Space-filling curves

Computer graphics studies offer a variety of practical and innovative space-filling curves that are relevant to this research. These methods generate constantly evolving patterns through simple rules, creating a space defined by curves rather than solids. For instance, the fractal algorithm can simulate natural shapes by adjusting the size and orientation of the basic shape (Smith, 1984) and can be applied to decorative patterns, porous structures, and virtual reality systems (Cui et al., 2011; Taylor, 2021; Ullah et al., 2021; Yang et al., 2008). The coral algorithm, inspired by the grooved surface of brain coral, can produce various porous shapes by manipulating the topology of Thiessen polygons (Zhai et al., 2013). This algorithm has already been utilized in the pavement of a 3DCP bridge (Xu et al., 2020). Besides, quad mesh generation is a method to subdivide a closed polygon into multiple well-organized quadrangles, which is considered a practical print path generation strategy (Wan et al., 2022). By incorporating guiding curves and attractor points inside the boundary, the organization of the quad mesh can be further modified to achieve dynamic pattern (Li et al., 2011; Wu et al., 2022b). In addition, other space-filling algorithms, like the vector field (Ichihara & Ueda, 2022) and the cracks pattern (Iben & O'Brien, 2009), are also suitable for 3DCP pavements.

Based on the design requirements of the 3DCP park, this study adopts the fractal algorithm, coral algorithm, and quad mesh generation algorithm as

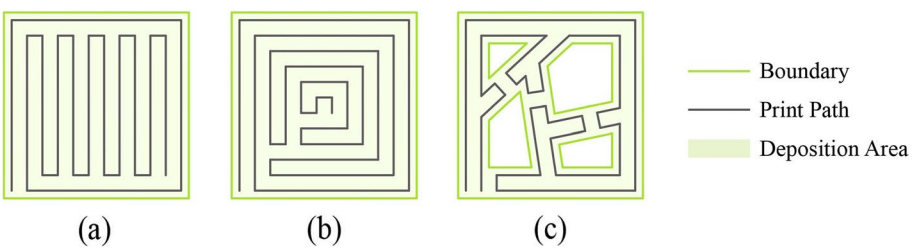

Fig. 2 The print path generation logics: **a** Zigzag path; **b** Contour-parallel path; **c** The print path generation intention for this study

space-filling methods to generate the basic pavement patterns (Section 3).

2.2.2 Print path generation rules

A fundamental principle for generating print paths in 3DCP is the continuous path (Bi et al., 2022; Gomez et al., 2022). This refers to a print path that is a smooth, uninterrupted curve comprising the path for each print layer and the line segments connecting interlayer spaces. Specifically, there are three interlayer connection scenarios to ensure the continuous path (Fig. 3):

(1) Loop path: When the print path can form a close loop in each layer, the end of the current layer could become the start of the next layer, and the connection position between layers can always occur at the same place (Yuan et al., 2022b).
(2) Retracing path: When the print path has two distant endpoints, the end of the current layer can only be connected vertically with the end of the next layer, and the next layer should be printed in the opposite direction (Wan et al., 2022).
(3) Alternate path: In this case, although the endpoints of each print path are separate, they can connect directly to the boundary of each layer. Thus, two different print paths can be designed according to the different positions of the endpoints, and these two paths should be stacked alternately to construct the entire print path (Biegler et al., 2020).

In addition to the above rule, it's essential to adhere to specific 3DCP requirements to achieve optimal printing quality. Firstly, avoiding self-intersection and sharp turning points in the print path can help to prevent overfilling and achieve a uniform distribution of concrete inks (Wan et al., 2022). Secondly, it is essential to minimize printing errors caused by uneven topography. For in-situ printing, the topography must be measured in advance so that the undulation of the print path can be adjusted to match the ground. For prefabrication, a leveling layer should be printed on the floor to eliminate height differences, creating a precise plane within the production area. Besides, to create different design scenarios, designers often integrate 3DCP with other construction processes (e.g., material-pouring, planting, assembling) and have additional requirements for the print path. In this study, these additional requirements are listed in Tables 2 and 3 with elaborations in Sections 3 and 4.

3 Space-filling methods

This section will introduce three kinds of space-filling curves and their generation methods. From the subjective side, the selections of these curve generation methods need to echo the landscape design images: the river, the coral, and the cloud. From the objective side, these curves also need to meet the additional printing or construction requirements brought by the corresponding pavement types:

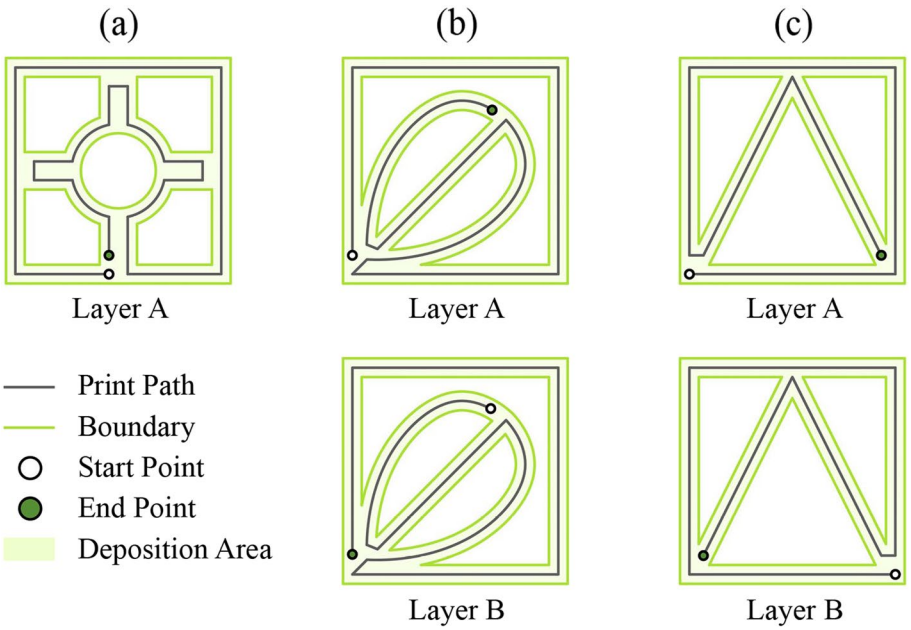

Fig. 3 Print path connection scenarios to ensure continuous contour: **a** Loop path; **b** Retracing path; **c** Alternate path

(1) The river pavement will be poured with terrazzo, so the space in-between adjacent print paths should be wide and continuous, ensuring a convenient pouring process. If the print paths are all gathered at certain endpoints, or there are too many intersections among print paths, it will result in a lot of sharp corners which is not easy to be poured with terrazzo. Therefore, flow-shape patterns like the field lines and the strange attractors are excluded from the design options.
(2) The coral pattern functions as permeable grass paving. Namely, turfs need to be planted in the cells of the coral shape. Considering that the size of the turf is fixed, the hexagonal grid is adopted as the prototype of the space-filling pattern to facilitate the planting process.
(3) The cloud pattern, inspired by the Chinese traditional Auspicious Clouds Motif (Sturman, 1990; Xue, 2021), will be filled with cold asphalt. Although the pattern is design-oriented, the gaps between printed paths should also be wide and continuous, allowing the cold asphalt to fully fill the space. To achieve this, a new space-filling pattern with the Auspicious Clouds flavor is developed utilizing the fractal algorithm.

Based on the above considerations, the generation requirements, basic algorithms, and optimization goals for these space-filling curves can be introduced in Table 1.

3.1 River pattern space-filling methods

To create the flow pattern for the river pavement, the quad mesh subdivision method was chosen. This approach subdivides a surface based on its boundaries and guiding curves, which is suitable for generating meshes that align with the provided boundaries. The river pavement has two predefined design elements: the boundary and the landscape islands in the central square. Hence, the goal of the space-filling process is to generate the organic flow by just using these elements (Fig. 4). Firstly, we connect the nearest points among all curve pairs and then select the shortest connection for each curve. This step converted the topology of the porous shape into multiple homogeneous and easy-to-subdivide geometries. Secondly, Bezier curves (Elber, 1992) were created based on the normal vectors of each element at the intersection point. Finally, the Bezier curves were used as the reference curve to generate quad meshes, resulting in a mesh with organic flowing features.

To extract the flow pattern from the meshes, a series of methods are employed (Fig. 5). The initial step is to select line segments that follow the direction of the river. To achieve this, the site boundary line is converted into three sets of continuous vectors, and the mesh segments are classified based on their distances to these vectors. As shown in Fig. 5b, mesh segments adjacent to the same vector are marked as one category. Next, using the vector angle formula $(\theta = cos^{-1}[(\overline{a} \cdot \overline{b})/(|\overline{a}| \cdot |\overline{b}|)])$, the angle between each mesh segment and its corresponding boundary vector is calculated. Segments with angles within a specific range are then selected to form the flow patterns of the river. To add a dynamic trend to the flow, the last step involves interfering with the flow pattern using randomly generated attractors.

Table 1 Requirements, algorithms, and optimization goals for space-filling curves

Type	Function	Requirement	Basic Algorithm	Optimization Goal
River	Terrazzo paving	Wide and continuous in-between space	Quad Mesh	Organic flow
Coral	Grass paving	Controllable cell sizes for grass planting	Voronoi, Hexagonal grid	Irregular shape
Cloud	Asphalt paving	Wide and continuous in-between space	Fractal	Continuous curve

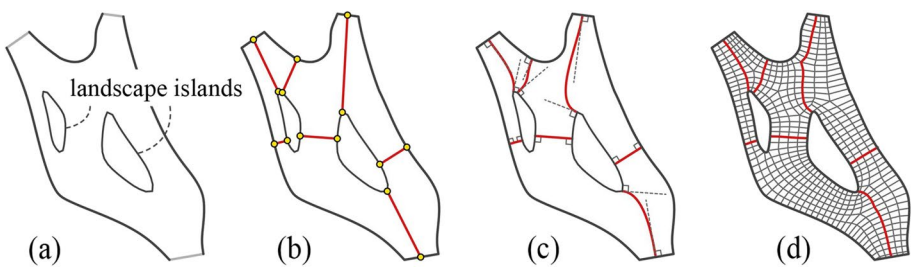

Fig. 4 The quad mesh generation process of the central square: **a** Predefined boundaries in the master plan; **b** Select the shortest connection among curve pairs; **c** Convert the shortest connections into Bezier curves; **d** Quad meshes with organic flowing features

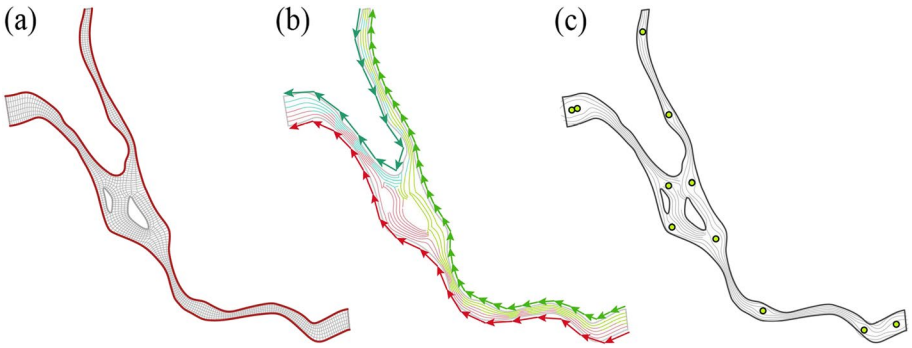

Fig. 5 The flow pattern extraction process: **a** Select the boundary of the river pavement; **b** Screen flow pattern according to the boundary vectors; **c** Enhance the dynamic of flow pattern by attractors

3.2 Coral pattern space-filling methods

The Voronoi algorithm (Voronoi, 1908a, b) is developed to create permeable pavements that mimic the irregular grooved surface of brain coral. While previous studies have investigated brain coral's forming mechanisms for environmental restoration (Lin et al., 2023) or CFD-optimized design (Wits et al., 2018), these bionic methods tend to be computationally intensive when generating large-area print paths. In contrast, this paper proposes a more practical approach for 3DCP (Fig. 6). First, the Voronoi algorithm generates irregular polygons that define the shape of each component over the entire paving area. Next, a lattice is evenly distributed in each component based on hexagonal grids. Then, random vectors are provided to disturb the matrix and convert the regular hexagonal grid into an irregular one. To imitate the penetration and combination mechanism of the brain coral surface, we allow designers to input a specific length range when generating coral shapes. Accordingly, edges within this range will be removed to form a larger polygon. Using this principle, porous structures of different sizes and topological logic can be created in each component, serving as a reference for print path generation.

3.3 Cloud pattern space-filling methods

The cloud pattern is produced using an optimized fractal algorithm. We aim to replace the polylines of the fractal algorithm with irregular curves, ensuring a continuous and smooth cloud pattern. To achieve this, the Gosper Curve (Gardner, 1976) is selected as the reference (Fig. 7). This curve can be evenly distributed in a hexagonal grid with the same spacing and without self-intersection.

The optimization of the fractal algorithm needs to consider two factors at the same time, vector direction and subdivision region. On the one hand, the vector direction is the guild line of the fractal process. As shown in Fig. 7, in fractal graphics, each basic type includes not only the length and position of the line segment but also the

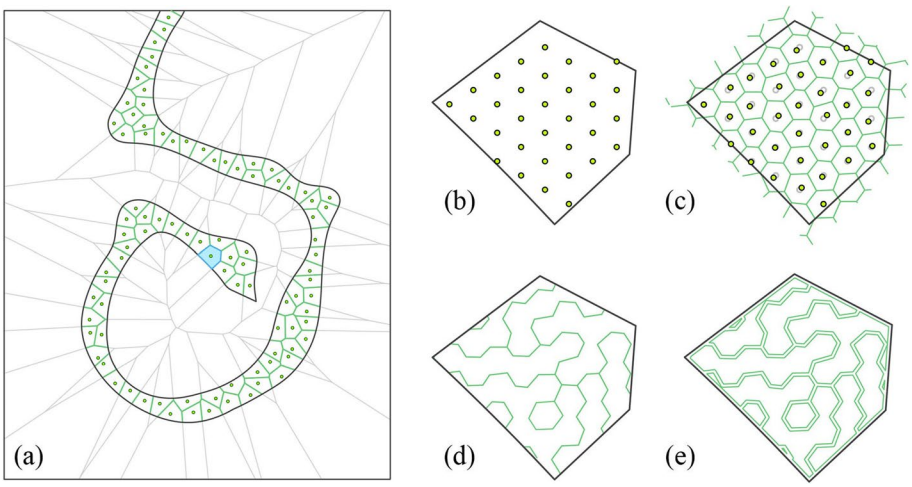

Fig. 6 Brain coral pattern generation process: **a** Thiessen polygons generation, a polygon example (marked blue) is selected to demonstrate the coral pattern generation process; **b** Hexagonal lattice generation; **c** Irregular hexagonal grid generation; **d** Merge adjacent hexagons by a specific length range; **e** Offset the pattern for print path generation

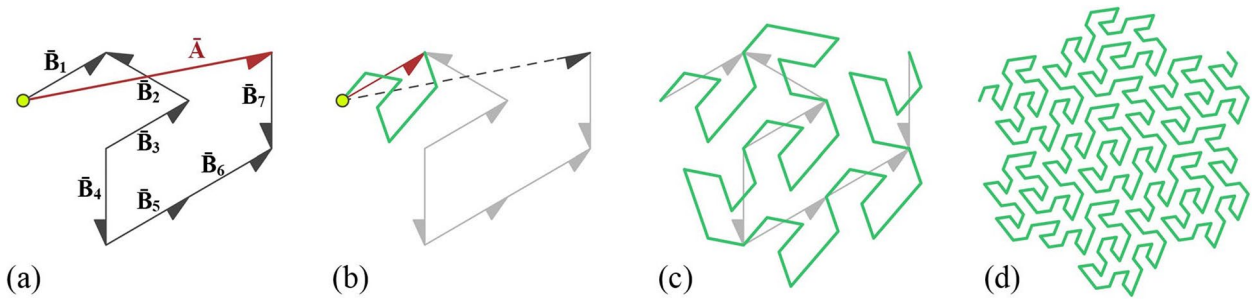

Fig. 7 The Gosper Curve generation mechanism: **a** The overall direction (Vector A) and specific directions (Vector B_1 to B_7); **b** Reorient the shape from Vector A to Vector B_1; **c** Fractal shape after the first iteration; **d** Fractal shape after the second iteration

overall direction of the basic pattern (vector A) and the specific direction of each line segment (vector B_1 to B_7). The fractal process can be considered as reorienting the basic pattern from vector A to each vector B. Therefore, when replacing line segments, no matter how complex the curve is, the endpoints and direction of the curve should be consistent with the original direction of each segment.

On the other hand, the subdivision region is defined to avoid the self-intersection issue of the curve after replacement. As shown in Fig. 8a, the hexagonal grid can divide the Gosper Curve into several independent regions (Gardner, 1976; Uher et al., 2019), in which there is only one basic unit within the boundary. Replacing the curve within the hexagonal region can ensure that the new pattern will not intersect itself. However, as shown in Fig. 8e, the boundary of the hexagonal grid is actually very close to segment 1 and segment 7, which means that there are few alternative patterns for these two segments. In contrast, segments 5 and 6 are far away from the boundary, so we consider changing the boundary of the hexagonal grid based on mosaic rules (Fig. 8f-g), transferring the additional space of segments 5 and 6 to segments 1 and 7, and then applying cloud curves within the new subdivision region (Fig. 8h).

Notably, the goal of defining and optimizing the subdivision region is to verify whether the final cloud curve will have a self-intersection issue. Hence, the cloud curve

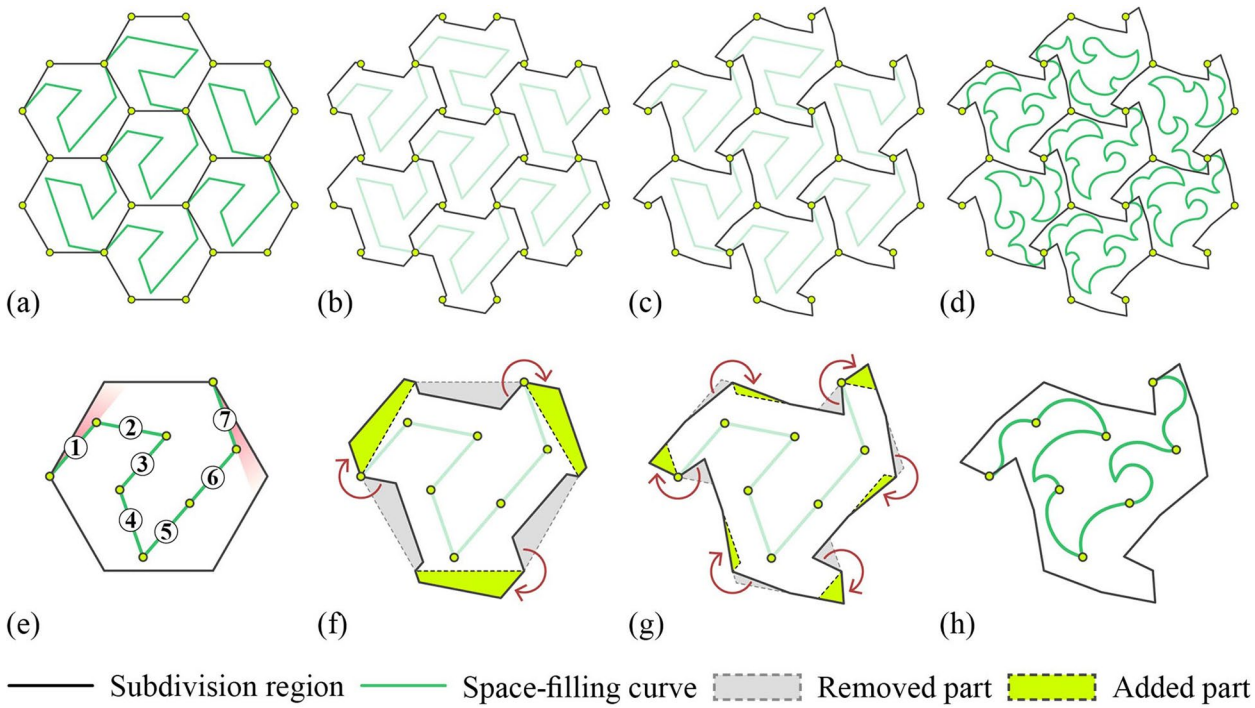

Fig. 8 **a**-**d** The pattern-replacing process; **e**-**h** The subdivision region optimization process

only needs to keep within the boundary of the subdivision region, while its proximity to the boundary is not a criterion to evaluate the resulting curve. The proximity requirement only plays a role in the boundary optimization process (Fig. 8f-g), in which the subdivision region is changed while the Gosper curve is not. In the boundary optimization process, the original Gosper curve is the reference to evaluate whether the optimized boundary is far away enough from segment 1 and segment 7. If so, there are more design options available to replace the original curve. In Fig. 8, only (h) is the result of the replacement. Similar to (e), even if there are segments extremely close to or far away from the boundary, the new curve can be evenly distributed on the plane once the boundary is removed.

4 Print path generation methods

The purpose of this section is to convert the space-filling curves into printable paths suitable for 3DCP. The methods employed adhere to the interlayer connection rules outlined in Section 2.2.2 and address the construction requirements associated with the pavements (Table 2).

4.1 River print path generation

The main challenge to generate the river print path is to match the topography. As the only impervious paving in the master plan design, the river pavement plays the role of surface water diversion and therefore has a great height difference. Accordingly, the priority of the river print path generation is that the path needs to fit the topography as much as possible. In addition, considering that the river pavement has a unique topology with a large central square and three long pathway branches (Fig. 5), we choose both in-situ printing (for the central square) and prefabrication (for the pathway) to construct the pavement. So, the generation methods of the print path should fit these two printing modes respectively.

In order to solve the above problems, we propose two positioning methods: robotic arms positioning and extreme points positioning. In in-situ printing, the robotic arms positioning method is adopted to ensure a good match between the print path and the concrete blinding. The concrete blinding is a pre-poured concrete base, which provides a stable working surface to support both the in-situ robots and 3DCP components. We installed and positioned the robotic arms in the central square, and then let the print head randomly touch multiple positions on the surface of blinding. Recorded by Euler angles, the robot poses of each touch were input into the KUKA|prc (Braumann & Brell-Cokcan, 2011), a grasshopper plugin, to recover these points in the digital model. Subsequently, an actual topography of the blinding was generated based on these points. Then the river print path was projected onto the digital blinding surface, realizing a good match between the virtual and real world.

Table 2 Interlayer connection rules and requirements for print paths

Type	Interlayer Connection	Requirement
River	Loop Path	Match the uneven topography
		Meet assembly requirements
Coral	Alternate path	Generate continuous path for porous shapes
		Avoid stack bond and vertical crack
Cloud	Retracing path	Subdivide complex continuous curve
		Component size control

The extreme points positioning method is utilized in the prefabrication works. Since the workspace is flat in the prefabrication shed, three-dimensional curves cannot be printed without the formwork or a preprinted curve base, which can make the prefabrication process time- and material-consuming. Therefore, the print path for prefabrication is better to have a flat bottom (Yuan et al., 2022a). Specifically, we extract the extreme points of each prefabrication component and construct a vector by these points. Then both the reference plane and projection direction can be constructed based on the cross-product of the provided vector and the X-axis. Subsequently, by projecting the river print path along the projection direction onto the reference plane, a flat print path close to the three-dimensional model can be generated (Fig. 9).

Besides the positioning issue, the river pavement still needs to meet various design and construction requirements, including pouring, transportation, and curb generation (Fig. 10). Based on the landscape design, the river pavement should be filled with terrazzo. To ensure that the printed river shape can better withstand the side thrust brought by the pouring process, the bottom of the river shape is strengthened by parallel print paths. Moreover, to make the component suitable for transportation and assembly, horizontal trusses are also integrated into the bottom river shape. The print path continues after the river shape is completed, forming the curb between the landscape and pavement. Correspondingly, the start point of the river print path should locate within the projection region of curbs, so as to ensure the continuity of the print path.

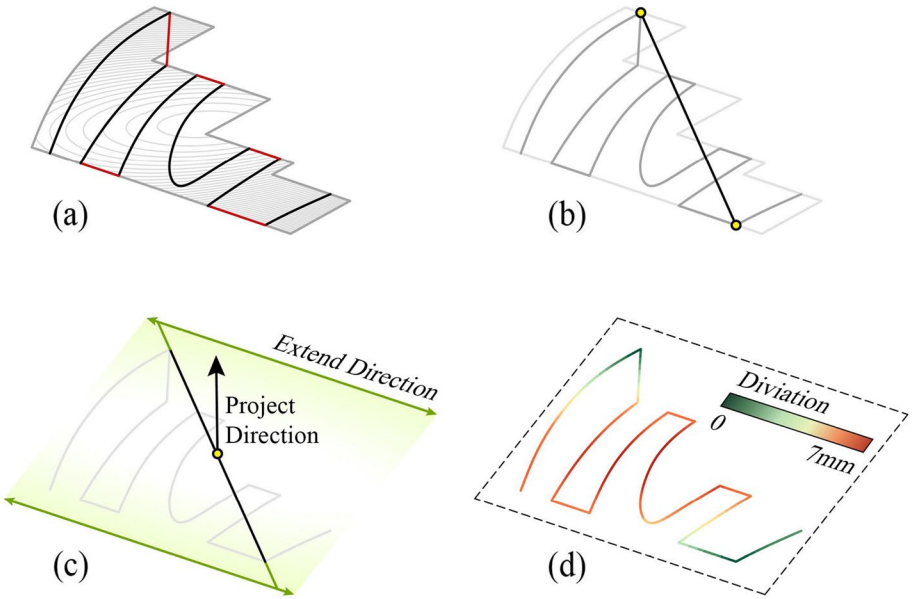

Fig. 9 Extreme points positioning method: **a** A three-dimensional component for the river pattern; **b** Find and connect extreme points; **c** Generate the reference plane and projection direction; **d** Project the river pattern onto the reference plane

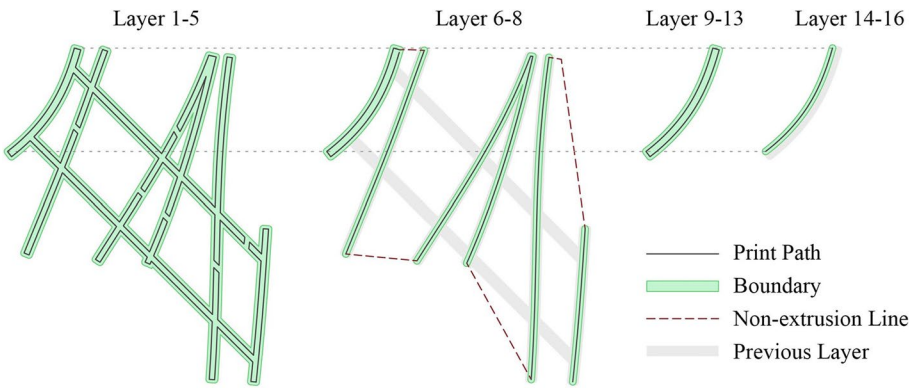

Fig. 10 River print path generation process

4.2 Coral print path generation

The coral print path generation methods aim to meet the continuous path requirement and avoid the stack bond issue. On the one hand, we need to outline all the irregularly distributed porous shapes by a continuous curve without self-intersection. On the other hand, in order to improve the structural integrity of each component, it is necessary to avoid the stack bond in the component to eliminate the potential vertical crack during transportation and usage. The stack bond issue happens in the position where short print paths are used to bridge two adjacent shapes (Fig. 11), since the "bridge" exists in the same position on each layer, that can result in a weak bond similar to the stack bond issue of the brick wall. To avoid such situations, we hope the "bridges" of adjacent layers exist in different positions, which requires that at least two print path scenarios should be generated for each component.

The adjacent points random retrieval method is utilized to solve the above generation challenges (Fig. 12). We first randomly select a polygon (H_0) in the porous shape and retrieve one random point (P_1) from the line segments closest to H_0. H_0 can then be connected with the other polygon where P1 is located (H_1). A similar connection logic can be operated several times until all polygons can be connected as a whole, which is a continuous curve without self-intersection. Since the selections of the initial polygon and closest point can

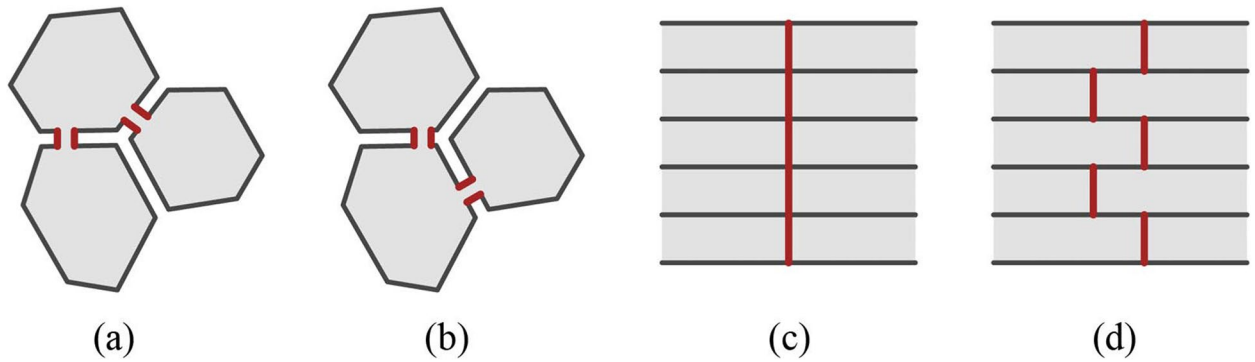

Fig. 11 **a**-**b** Two different connection scenarios for porous shape (red lines are the short print path to bridge adjacent polygons); **c** Section of the 3DCP shape with the stack bond issue (using just one connection scenario); **d** Section of an ideal 3DCP shape (stacking two different connection scenarios)

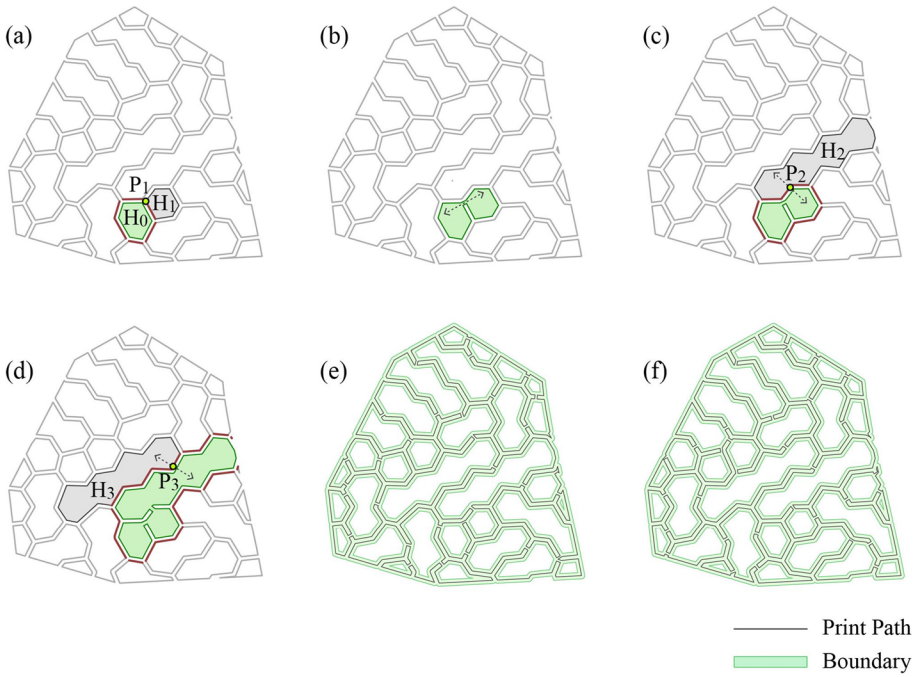

Fig. 12 The adjacent points random retrieval method: **a** Randomly retrieve a polygon and an adjacent point; **b** Bridge adjacent polygons; **c** The second iteration of the same retrieval process; **d** The third iteration; **e** The generation result; **f** Another result generated by a different initial polygon

be different and random, the connection results are diverse. Two different schemes can be selected among the results, and they can be weaved together to form the print path that doesn't have the stack bond issue.

4.3 Cloud print path generation

The difficulty in generating the cloud print path lies in how to cut the continuous fractal curve within a given boundary and how to subdivide the curve into components with appropriate dimensions. If a fixed boundary is used to cut the cloud curve without following its topology, it can result in lots of curve segments. To avoid this problem, the midpoints of the Gosper curve are utilized as the index to define which part of the cloud curve should be selected (Fig. 13). Specifically, a rough boundary is drawn in the Gosper curve, then the line segments with their midpoints inside the boundary are selected. Subsequently, these line segments are replaced by the corresponding cloud curves, forming the cloud pavement with a blur and organic boundary.

The cloud print path generation method follows the process of "join-subdivision-reorientation", which

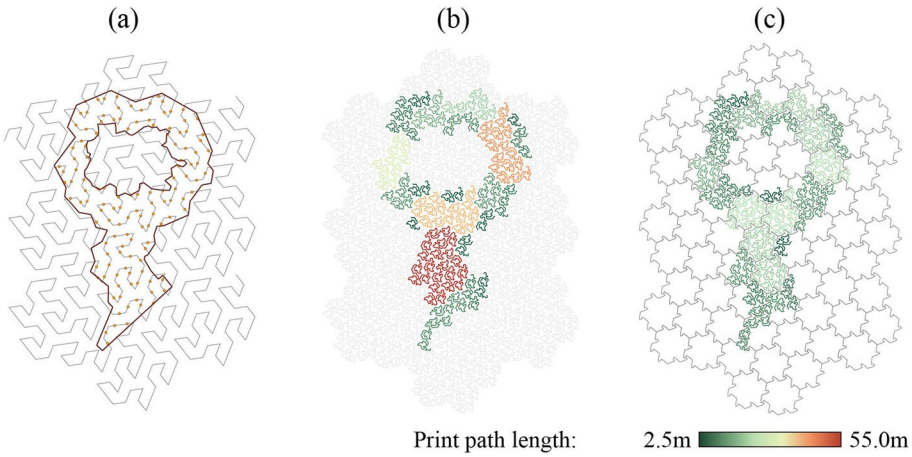

Fig. 13 Cloud print path generation process: **a** Screen available segments by the location of their midpoints; **b** Generate and join the cloud curves; **c** Subdivide the cloud curves into transportable sizes

ensures that the sizes of the components are all within a suitable range including 3–9 cloud units (Figs. 13 and 14). Firstly, all the cloud curves are joined to form as large a component as possible (each component still consists of only one continuous curve). Secondly, these large components are subdivided by the mosaic pattern generated in Section 3.3, so that the size of each component does not exceed 7 cloud units. Thirdly, the small components containing only 1 or 2 cloud units are reoriented and joined with other components (Fig. 14).

5 Results

5.1 Construction outcome

The construction consisted of two parts, the in-situ printing of the central square and the prefabrication of other components in a temporary shed located beside the site.

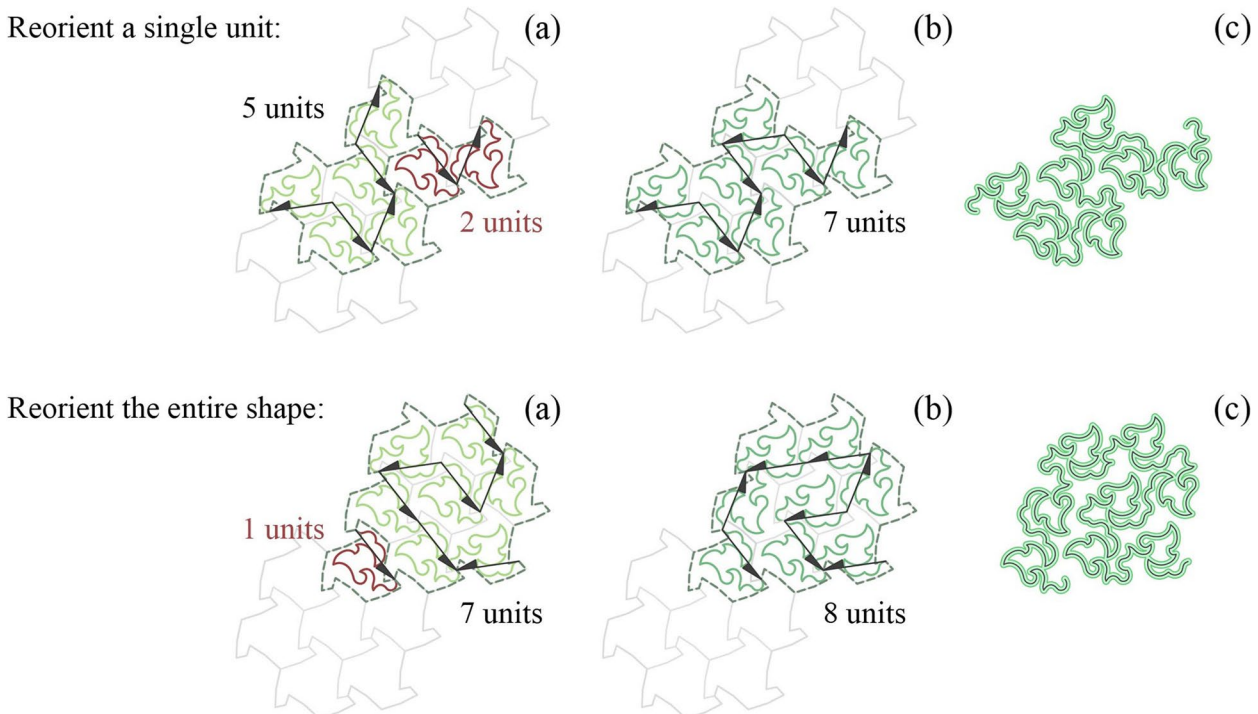

Fig. 14 Reorientation process: **a** Examples of small components with only 1 or 2 cloud units; **b** Reorient a single unit or the entire component to incorporate the adjacent curve; **c** Print path generation results

Starting from the in-situ works, we used four KUKA robotic arms to print the central square river pavement simultaneously. Then the robotic arms were relocated to the shed to accomplish independent tasks.

Different construction workflows were assigned to these pavements according to the landscape design requirements. After the river pavement was assembled on the concrete blinding, coarse aggregate concrete was poured in between the concrete strips. Then we smoothed the entire surface after the concrete was cured, presenting the texture of terrazzo. Coral pavements were used as the permeable pavement of the park, which are assembled above a soil blinding. The porous shapes of the coral pattern were then filled with the greensward to achieve a cohesive presentation with the surrounding landscape. The cloud pavement was also constructed on the grass to guide visitors to an iconic sign sculpture of the park. Therefore, we use cold asphalt as a filler to achieve a flat surface with high accessibility. The construction results of all types of pavement are presented in Fig. 15.

5.2 Discussion

The design-to-construction process of these pavements also reveals topics that are worth further discussion. Such as the size control issue of the 3DCP component. Since the space-filling curves emphasize design complexity rather than structure performance, a large and flat component could be fragile in the transportation and assembly process, which sometimes needs to be reprinted. Based on the actual assembly experience, small 3DCP pavement components (with the longest diameter smaller than 1.5 m) present better structural stability in the assembly process than larger ones. That's because the assembly process involves several steps of tiny movement to precisely position each component, while large-size components, with larger weight as well as lower flexibility, have a higher risk of being over-moved and being

Fig. 15 Construction process and outcome of the Shenzhen Baoan 3D printing park (Sources: XWG Design Studio): **a** The river pavement; **b** The coral pavement; **c** The cloud pavement

Table 3 The challenges and solutions in this study

Type	Workflow	Challenges	Solutions
River	Space-filling	Generate dynamic flow pattern	(1) Generate quad mesh based on boundaries' normal vectors (2) Extract mesh segments based on boundaries' tangent vectors
	Printing	Match print path with uneven topography	(1) For in-situ printing: Survey the topography by robots (2) For prefabrication: Apply the extreme points positioning method
	Assembly	Enhance component base	For prefabrication: (1) Generate parallel print paths (2) Add horizontal trusses
Coral	Space-filling	Generate irregular porous shape	(1) Generate hexagonal Voronoi diagram (2) Combine hexagons based on their edge lengths
	Printing	Ensure continuous print path	Apply the "adjacent points random retrieval method"
	Assembly	Address stack bond issue	Provide two print path schemes using different initial hexagons
Cloud	Space-filling	Define the pavement boundary	Screen available Gosper curve segments by their midpoints' location
	Printing	Avoid self-intersection	Optimize the subdivision region based on the mosaic rule
	Assembly	Control component size	Follow the "Join-subdivision-reorientation" workflow

cracked by the collision with other objects (e.g., hard surface, assembled component, concrete blinding). Besides controlling the size of all components, other practical solutions are to increase the print width or print path density at the edge of the large component, making it stronger to withstand unexpected collision, or reduce the weight of the component by topological optimization (Xia et al., 2023), making it lighter to lower the chance of being over-moved.

In addition, the construction process of river pavement proves that the construction efficiency of in-situ printing is much higher than that of prefabrication. The in-situ printing of the central square took only 1 day, while it took nearly 1 week for the rest of the river pavement to be printed and installed. Most of the time was spent on the positioning and assembling process. It is worth mentioning that, in this project, the in-situ printing and the prefabrication have nearly equal time costs in terms of robot set-up, because the in-situ printing works of the central square can be printed in one go without repositioning the robots. However, if the entire project is constructed by in-situ printing, additional site survey and repositioning steps will be involved. Therefore, the in-situ printing method based on fixed robotic arms is more suitable for the pavement with a large and concentrated area like the central square. For the narrow trails in the park, the cost of repositioning the robot arm will significantly exceed the benefits brought by in-situ printing. Therefore, despite the longer production and assembly duration, prefabrication becomes the only choice for trail pavements. In the future, small and mobile 3D printing devices, such as drones (Zhang et al., 2022) and grip robots (Jokic et al., 2014), will be more efficient options for large-format 3D printing projects as they have better movability and flexibility to tackle different construction conditions.

Finally, the design-to-construction processes of these pavements all follow the workflow of "space-filling, printing, assembly". Correspondingly, the challenges and solutions in this 3DCP pavement study can be summarized in Table 3.

6 Conclusion

Pavement design emphasizes the use of simple rules to generate logical but constantly changing patterns, which provides an approach to combining math with aesthetics. Utilizing 3DCP as a construction method, this study proves the feasibility of various pavement generation methods in large-scale landscape design. The value of this study can be summarized as follows:

(1) Provide practical space-filling and print path generation methods, which have the potential to improve the programming efficiency for complex 3DCP geometries and can be applied to other projects.
(2) Adopt and optimize classical curve pattern generation algorithms to achieve a 3D printing area significantly larger than that of current LFAM practices.
(3) Summarize the problems that may occur in designing and constructing 3DCP pavements, and put forward feasible solutions;
(4) Present the design options of combining 3DCP with different landscape elements and construction materials;
(5) Introduce a standard print path generation workflow for each pavement type to realize non-standard outcomes, promoting the benefits of 3DCP in combining automation and customization.

Acknowledgements
The authors would like to thank the design and research team members who were involved in the project: Yuan Gao, Chenwei Sun, Zhi Wang, Fang Cui, Yuting He, Zhipeng Lin, Yudong Yin, Yuanxu Zhuang, Zhiling Zhang, Yue Mei, Yuxuan Mao, Xiayu Zhao, Yinhang Han.

Authors' contributions
Conceptualization: Shuyi Huang and Weiguo Xu; Methodology and formal analysis: Shuyi Huang; Supervision: Weiguo Xu; Visualization and writing – original draft: Shuyi Huang and Hanyang Hu; Writing – review & editing: Shuyi Huang. All authors have read and agreed to the published version of the manuscript.

Funding
This research was funded by Shenzhen International Graduate School, Tsinghua University.

Availability of data and materials
Data sharing is not applicable to this article as no datasets were generated or analyzed during the current study.

Declarations

Competing interests
The author Weiguo Xu is the member of Editorial Board for Architectural Intelligence but were not involved in the journal's review, or any decisions, related to this submission.

Received: 31 March 2023 Accepted: 2 June 2023
Published online: 29 June 2023

References

Anton, A., Reiter, L., Wangler, T., Frangez, V., Flatt, R. J., & Dillenburger, B. (2021). A 3D concrete printing prefabrication platform for bespoke columns. *Automation in Construction*, *122*, 103467. https://doi.org/10.1016/j.autcon.2020.103467

Bi, M., Xia, L., Tran, P., Li, Z., Wan, Q., Wang, L., Shen, W., Ma, G., & Xie, Y. M. (2022). Continuous contour-zigzag hybrid toolpath for large format additive manufacturing. *Additive Manufacturing*, *55*, 102822. https://doi.org/10.1016/j.addma.2022.102822

Biegler, M., Wang, J. H., Kaiser, L., & Rethmeier, M. (2020). Automated tool-path generation for rapid manufacturing of additive manufacturing directed energy deposition geometries. *Steel Research International*, *91*(11), 2000017. https://doi.org/10.1002/srin.202000017

Braumann, J., & Brell-Cokcan, S. (2011). Parametric robot control: Integrated CAD/CAM for architectural design. In *Proceedings of the 31st Annual Conference of the Association for Computer Aided Design in Architecture (ACADIA)* (pp. 242–251). ACADIA. https://doi.org/10.52842/conf.acadia.2011.242

Cui, H., Qi, M., & Li, D. (2011). 3D cloud modeling base on fractal particle method. In *Proceedings of 2011 International Conference on Electrical and Control Engineering (ICECE)* (pp. 5639–5643). IEEE. https://doi.org/10.1109/ICECENG.2011.6057499

Duty, C. E., Kunc, V., Compton, B., Post, B., Erdman, D., Smith, R., Lind, R., Lloyd, P., & Love, L. (2017). Structure and mechanical behavior of Big Area Additive Manufacturing (BAAM) materials. *Rapid Prototyping Journal*, *23*(1), 181–189. https://doi.org/10.1108/rpj-12-2015-0183

Elber, G. (1992). III.7 - Interpolation using Bezier curves. In D. Kirk (Ed.), *Graphics Gems III (IBM Version)* (pp. 133–136). Morgan Kaufmann. https://doi.org/10.1016/B978-0-08-050755-2.50037-3

Gardner, M. (1976). Mathematical games—In which "monster" curves force redefinition of the word "curve." *Scientific American*, *235*(6), 124–133. http://www.jstor.org/stable/24950510.

Gomez, G., Cortés, C., Creus, C., Amilibia, M. Z., & Moreno, A. (2022). Generation of continuous hybrid zig-zag and contour paths for 3D printing. *The International Journal of Advanced Manufacturing Technology*, *119*(11), 7025–7040. https://doi.org/10.1007/s00170-021-08418-z

Grasser, G., Pammer, L., Köll, H., Werner, E., & Bos, F. P. (2020). Complex architecture in printed concrete: The case of the Innsbruck University 350th Anniversary Pavilion COHESION. In *Proceedings of the Second RILEM International Conference on Concrete and Digital Fabrication* (pp. 1116–1127). Springer International Publishing. https://doi.org/10.1007/978-3-030-49916-7_106

Hu, S. J. (2013). Evolving paradigms of manufacturing: From mass production to mass customization and personalization. *Procedia CIRP*, *7*, 3–8. https://doi.org/10.1016/j.procir.2013.05.002

Huang, S., Xu, W., & Li, Y. (2022). The impacts of fabrication systems on 3D concrete printing building forms. *Frontiers of Architectural Research*, *11*(4), 653–669. https://doi.org/10.1016/j.foar.2022.03.004

Iben, H. N., & O'Brien, J. F. (2009). Generating surface crack patterns. *Graphical Models*, *71*(6), 198–208. https://doi.org/10.1016/j.gmod.2008.12.005

Ichihara, N., & Ueda, M. (2022). 3D-print infill generation using the biological phase field of an optimized discrete material orientation vector field. *Composites Part B: Engineering*, *232*, 109626. https://doi.org/10.1016/j.compositesb.2022.109626

Jokic, S., Novikov, P., Maggs, S., Sadan, D., Jin, S., & Nan, C. (2014). Robotic positioning device for three-dimensional printing. *arXiv preprint*, 1406.3400. https://doi.org/10.48550/arXiv.1406.3400

Krishnamurthy, V., Poudel, L., Ebert, M., Weber, D. H., Wu, R., Zhou, W., Akleman, E., & Sha, Z. (2022). LayerLock: Layer-wise collision-free multi-robot additive manufacturing using topologically interlocked space-filling shapes. *Computer-Aided Design*, *152*, 103392. https://doi.org/10.1016/j.cad.2022.103392

Li, Y., Wang, W., Ling, R., & Tu, C. (2011). Shape optimization of quad mesh elements. *Computers & Graphics*, *35*(3), 444–451. https://doi.org/10.1016/j.cag.2011.03.037

Lin, S., Chou, N., Bao, D., Zhang, G., Xiong, C., Fang, J., & Xie, Y. M. (2023). Design and fabrication of artificial brain coral: Evolution principle, turbulent hydrodynamics and matter interchange. *Computers & Structures*, *276*, 106955. https://doi.org/10.1016/j.compstruc.2022.106955

Ruelle, D., & Takens, F. (1971). On the nature of turbulence. *Communications in Mathematical Physics*, *20*(3), 167–192. https://doi.org/10.1007/BF01646553

Shen, H., Pan, L., & Qian, J. (2019). Research on large-scale additive manufacturing based on multi-robot collaboration technology. *Additive Manufacturing*, *30*, 100906. https://doi.org/10.1016/j.addma.2019.100906

Smith, A. R. (1984). Plants, fractals, and formal languages. *ACM SIGGRAPH Computer Graphics*, *18*(3), 1–10. https://doi.org/10.1145/964965.808571

Sturman, P. C. (1990). Cranes above Kaifeng: The auspicious image at the court of Huizong. *Ars Orientalis*, *20*, 33–68. https://www.jstor.org/stable/4629400.

Taylor, R. P. (2021). The potential of biophilic fractal designs to promote health and performance: A review of experiments and applications. *Sustainability*, *13*(2), 823. https://doi.org/10.3390/su13020823

Uher, V., Gajdoš, P., Snášel, V., Lai, Y.-C., & Radecký, M. (2019). Hierarchical hexagonal clustering and indexing. *Symmetry*, *11*(6), 731. https://doi.org/10.3390/sym11060731

Ullah, A. S., D'Addona, D. M., Seto, Y., Yonehara, S., & Kubo, A. (2021). Utilizing fractals for modeling and 3D printing of porous structures. *Fractal and Fractional*, *5*(2), 40. https://doi.org/10.3390/fractalfract5020040

Voronoi, G. (1908a). Nouvelles applications des paramètres continus à la théorie des formes quadratiques Deuxième mémoire. Recherches sur les parallélloèdres primitifs. *Journal für die reine und angewandte Mathematik (Crelles Journal)*, *1908*(134), 198–287. https://doi.org/10.1515/crll.1908.134.198

Voronoi, G. (1908b). Nouvelles applications des paramètres continus à la théorie des formes quadratiques. Premier mémoire. Sur quelques propriétés des formes quadratiques positives parfaites. *Journal für die reine und angewandte Mathematik (Crelles Journal)*, *1908*(133), 97–102. https://doi.org/10.1515/crll.1908.133.97

Wan, Q., Wang, L., & Ma, G. (2022). Continuous and adaptable printing path based on transfinite mapping for 3D concrete printing. *Automation in Construction*, *142*, 104471. https://doi.org/10.1016/j.autcon.2022.104471

Wits, W. W., Jafari, D., Jeggels, Y., Velde, S. v. d., Jeggels, D., & Engelberts, N. (2018). Freeform-optimized shapes for natural-convection cooling. In *Proceedings of the 2018 24rd International Workshop on Thermal Investigations of ICs and Systems (THERMINIC)* (pp. 1–6). IEEE. https://doi.org/10.1109/THERMINIC.2018.8593305

Wu, H., Li, Z., Zhou, X., Wu, X., Bao, D., & Yuan, P. F. (2022a). Digital design and fabrication of a 3D concrete printed funicular spatial structure. In *POST-CARBON - Proceedings of the 27th Computer-Aided Architectural Design Research in Asia (CAADRIA 2022a)* (pp. 71–80). CAADRIA. https://doi.org/10.52842/conf.caadria.2022.2.071

Wu, M., Wang, X., Nkonga, B., Mourrain, B., Xu, G., Ni, Q., & Liu, Y. (2022b). Flux-aligned quad mesh generation in magnetohydrodynamic simulation. *Journal of Computational Physics*, *466*, 111393. https://doi.org/10.1016/j.jcp.2022.111393

Xia, L., Bi, M., Wu, J., Wang, F., Wang, L., Xie, Y. M., & Ma, G. (2023). Integrated lightweight design method via structural optimization and path planning for material extrusion. *Additive Manufacturing*, *62*, 103387. https://doi.org/10.1016/j.addma.2022.103387

Xu, W., Gao, Y., Sun, C., & Wang, Z. (2020). Fabrication and application of 3D-printed concrete structural components in the Baoshan Pedestrian Bridge Project. In J. Burry, J. Sabin, B. O. B. Sheil, & M. Skavara (Eds.), *Fabricate 2020* (pp. 140–147). UCL Press. https://doi.org/10.2307/j.ctv13xpsvw.22

Xu, W., Zhang, Y., Gao, Y., & Sun, C. (2022). Robot 3DP technology applied in public garden construction: An introduction to Shenzhen Baoan 3DP Public Garden as an experimental project (in Chinese). *Architecture Technique*, *28*(07), 82–85. https://doi.org/10.19953/j.at.2022.07.006

Xue, F. (2021). *Rising clouds at water's edge: Clouds and mist in the Chinese imagination* [Master thesis, University of Virginia]. University of Virginia Library. https://doi.org/10.18130/0d8h-c755

Yang, L., Zhang, Y., & Li, H. (2008). Decorative pattern design of ceramic based on cloud model and fractal art. In *Proceedings of the 2008 9th International Conference on Computer-Aided Industrial Design and Conceptual Design* (pp. 890–894). IEEE. https://doi.org/10.1109/CAIDCD.2008.4730704

Yuan, P. F., Beh, H. S., Yang, X., Zhang, L., & Gao, T. (2022a). Feasibility study of large-scale mass customization 3D printing framework system with a case study on Nanjing Happy Valley East Gate. *Frontiers of Architectural Research*, *11*(4), 670–680. https://doi.org/10.1016/j.foar.2022.05.005

Yuan, P. F., Zhan, Q., Wu, H., Beh, H. S., & Zhang, L. (2022b). Real-time toolpath planning and extrusion control (RTPEC) method for variable-width 3D concrete printing. *Journal of Building Engineering*, *46*, 103716. https://doi.org/10.1016/j.jobe.2021.103716

Zhai, B., Xu, W., & Huang, W. (2013). Research on landscape system based on morphological structure of brain coral: Taking the landscape design of Tuancheng Lake area outside summer palace as an example (in Chinese). *Urbanism and Architecture*, *123*(19), 46–49. https://doi.org/10.19892/j.cnki.csjz.2013.19.014

Zhang, K., Chermprayong, P., Xiao, F., Tzoumanikas, D., Dams, B., Kay, S., Kocer, B. B., Burns, A., Orr, L., Choi, C., Darekar, D. D., Li, W., Hirschmann, S., Soana, V., Ngah, S. A., Sareh, S., Choubey, A., Margheri, L., Pawar, V. M., … Kovac, M. (2022). Aerial additive manufacturing with multiple autonomous robots. *Nature*, *609*(7928), 709–717. https://doi.org/10.1038/s41586-022-04988-4

Publisher's Note